Mechanical properties and force field parameters for polyethylene crystal

ARTICLE *in* THE JOURNAL OF PHYSICAL CHEMISTRY · MARCH 1991

Impact Factor: 2.78 · DOI: 10.1021/j100159a031

3 AUTHORS, INCLUDING:

Siddharth Dasgupta
California Institute of Technology
54 PUBLICATIONS **3,140** CITATIONS

SEE PROFILE

William A. Goddard
California Institute of Technology
1,333 PUBLICATIONS **68,233** CITATIONS

SEE PROFILE

detected by using a contemporary high-resolution interferometric spectrometer or tunable probe laser. The contemporary theory of the normal and anomalous Zeeman effect is adequately described, for example, on pp 243ff of Atkins.[26] In that theory we formally replace **m** by α_s and the gyromagnetic ratio by γ_π. A magnetic field of the order of 1.0 T splits lines in the Zeeman effect by about 0.5 cm^{-1}. The same splitting would require a pump laser electric field strength in the range of 10^6 Volt m^{-1}, as discussed already. This can be achieved easily by Q switching and focusing. Synchronous detection techniques (lock-in amplifiers) may be employed to integrate the time-accumulated effect of the pulsed pump laser by interfacing with the lockin amplifier of the interferometric spectrometer.

Note that there is also broadening and splitting due to the well-known optical (or ac) Stark effect.[31-35] However, the latter depends on the real part of the dynamic polarizability, which is T positive and does not have an axial vector equivalent. In consequence the ac Stark effect can be observed with a pump laser that is not circularly polarized,[31-35] in contrast to the optical Zeeman effect, which can be observed *only with a circularly polarized laser*. The differences between the optical Stark and Zeeman effects are as fundamental as those between the conventional Stark and Zeeman effects, induced respectively with a static electric and magnetic field. In the optical Zeeman effect there should also be the equivalent of the Paschen-Back effect, an anomalous optical Zeeman effect as the optical conjugate product is increased. In diatomics and polyatomics in which there is net electronic angular momentum, the Hund coupling models can be used to describe the various patterns as in Townes and Schawlow, chapter 11.[36]

This is a relatively straightforward "first experiment", which would reveal the degree of pump laser stability needed for a the second type of experiment, in which the pump laser is used with the highly homogeneous magnet of a state-of-the-art NMR or ESR spectrometer. A simple Hamiltonian for this second type would be, for example

$$\Delta H = -\gamma_n \mathbf{I}\cdot\mathbf{B} - \tfrac{1}{2}\gamma_\pi \mathbf{J}\cdot\pi \quad (44)$$

where

$$\mathbf{J} = \mathbf{L} + 2.002\mathbf{S} \quad (45)$$

and I is the nuclear spin quantum number. In Landē form this is

$$\Delta H \doteq -\gamma_N\left[1 + \frac{I(I+1) - J(J+1)}{2J_{tot}(J_{tot}+1)}\right]\mathbf{J}_{tot}\cdot\mathbf{B} - \frac{\gamma_\pi}{2}\left[1 - \frac{I(I+1) - J(J+1)}{2J_{tot}(J_{tot}+1)}\right]\mathbf{J}_{tot}\cdot\pi \quad (46)$$

where

$$J_{tot} = J + I \quad (47)$$

is the total angular momentum quantum number. For $I \neq 0$, we have the selection rule, and the NMR pattern in the absence of π is split according to

$$\Delta M_{J_{tot}} = 0, \pm 1 \quad (48)$$

The splitting depends on the individual values of I and J, in analogy with the extra Landē splittings observed in the theory of the anomalous Zeeman effect.[26]

The question of the homogeneity of the factor E_0^2 from the circularly polarized pump laser may turn out to be critical from experiment one. If so, synchronous detection techniques from infrared radio frequency double resonance may be able to filter out the background noise in E_-^2, leaving the signal, using highly sophisticated state-of-the-art lockin amplifiers interfaced with controlling microcomputers as described for example in Figure 1 of ref 37 in the context of sub-Doppler resolution infrared radio frequency double resonance. Detailed experimental conditions are given in ref 37 and references therein.

Note Added in Proof. Since this manuscript was submitted the verification experiment of laser NMR has been initiated at Princeton University by Prof. W. S. Warren and co-workers.

Acknowledgment. This research was supported by the Cornell Theory Center, which receives major funding from the NSF, IBM, New York State, and Members of the Corporate Research Institute.

(31) Hanna, D. C.; Yuratich, M. A.; Cotter, D. *Non-Linear Optics of Free Atoms and Molecules*; Springer Verlag: New York, 1979; eq 2.59.
(32) Feneuille, S. *Rep. Prog. Phys.* **1977**, *40*, 1257.
(33) Whitley, R. M.; Stroud Jr., C. R. *Phys. Rev. A* **1976**, *14*, 1488.
(34) Delsart, C.; Keller, J.-C. *J. Phys., B* **1976**, *9*, 2769.
(35) Molander, W. A.; Stroud Jr., C. R.; Yeazell, J. A. *J. Phys. B* **1986**, *19*, L461.
(36) Townes, C. H.; Schawlow, A. L. *Microwave Spectroscopy*; McGraw-Hill: New York, 1955; Dover, New York, 1975.
(37) Hennequin, D.; Glorieux, P.; Arimondo, E.; Evans, M. W. *J. Chem. Soc., Faraday Trans 2* **1987**, *83*, 463.

Mechanical Properties and Force Field Parameters for Polyethylene Crystal

Naoki Karasawa, Siddharth Dasgupta, and William A. Goddard III*

Materials and Molecular Simulation Center, Beckman Institute (139.74),† California Institute of Technology, Pasadena, California 91125 *(Received: December 7, 1989; In Final Form: September 7, 1990)*

Crystal structures, phonon dispersion relations, and elastic constants of polyethylene crystal are calculated by using a new force field where the van der Waals parameters are selected on the basis of comparing these properties with experiment. The cell parameters and atomic coordinates are optimized simultaneously, and elastic constants and phonon bands are calculated by using analytic second derivatives at the optimized structure. Yield stresses and surface energies are obtained from calculations of the stress-strain relations in directions perpendicular to polymer chains.

I. Introduction

Given a force field (the analytical description of forces on all atoms in terms of the distances and angles in a structure), one can calculate a number of important properties of crystalline polymers—structure, elastic constants, yield stresses, vibrational (phonon) states, specific heat, free energy, etc. However, suitable force fields do not exist for most polymers of interest. Herein, we report a new force field suitable for polyethylene (PE) and other hydrocarbons using a systematic approach to developing force fields that should be applicable to other polymers of interest.

† Contribution No. 7903.

0022-3654/91/2095-2260$02.50/0

With the new force field we calculate the structure by optimizing the six unit-cell parameters simultaneously with the atomic coordinates for all atoms within the unit cell. Allowing all atomic coordinates to readjust, the elastic constants and phonon dispersion relations (lattice modes and intramolecular modes) are obtained at the optimized structure (from analytical second derivatives). The phonon states are then used to obtain thermodynamic properties. These calculated properties of polyethylene are compared with experimental values.

For the directions perpendicular to the polyethylene chains, we calculate the stress–strain relations for finite strains until the crystal fractures. This is used to obtain the yield stresses and ultimate stresses for PE crystals and to obtain the surface energies.

II. The Force Field

The energy expression involves valence (E_{val}) and nonbond (E_{nb}) interactions

$$E = E_{val} + E_{nb} \tag{1}$$

where E_{val} includes the terms arising from covalent bond formation and E_{nb} includes the long-range noncovalent interactions. Here we take the covalent terms

$$E_{val} = E_b + E_a + E_t + E_x \tag{2}$$

to include bond stretch (E_b), angle bend (E_a), dihedral angle torsion (E_t), and cross (E_x) terms, while the nonbond terms

$$E_{nb} = E_{vdW} + E_Q \tag{3}$$

consist of van der Waals (E_{vdW}) and electrostatic (E_Q) terms. Consistent with common practice, we exclude 1–2 (bond) and 1–3 (angle) nonbond interactions.

A. Valence Interactions. The valence interactions (2) are described by using the following expressions:

(i) Morse terms

$$E_{IJ} = D_b[e^{-\alpha_b(R-R_b)} - 1]^2 \tag{4}$$

where R is the length of bond IJ, R_b and D_b are the position and depth of the well, and $k_b = 2D_b\alpha_b^2$ is the force constant.

(ii) Cosine angle-bond terms

$$E_a = \tfrac{1}{2}C[\cos\theta - \cos\theta_a]^2 \tag{5}$$

where θ is the angle between bonds IJ and JK, θ_a is the equilibrium angle, and $k_\theta = C\sin^2\theta_a$ is the diagonal force constant.

(iii) Threefold torsion terms

$$E_t = \tfrac{1}{2}V_t(1 + \cos 3\phi) \tag{6}$$

where ϕ is the torsional angle for bonds IJ, JK, and KL ($\phi = 0$ corresponds to cis) and V_t is the barrier.

(iv) Bond–angle and bond–bond cross terms of the form

$$E_{ax} = D_1(\cos\theta - \cos\theta_a)(R_1 - R_{b1}) + D_2(\cos\theta - \cos\theta_a)(R_2 - R_{b2}) + k_{rr}(R_1 - R_{b1})(R_2 - R_{b2}) \tag{7}$$

associated with each angle term (5), where R_1 and R_2 are the lengths of the IJ and JK bonds, $k_{r\theta} = -D\sin\theta_a$ is the angle-stretch force constant, and k_{rr} is the stretch–stretch force constant.

(v) One-center angle–angle cross terms of the form

$$E_{1aa} = G(\cos\theta_{IJK} - \cos\theta_{aIJK})(\cos\theta_{IJL} - \cos\theta_{aIJL}) \tag{8}$$

where $k_{1\theta\theta} = G\sin\theta_{aIJK}\sin\theta_{aIJL}$ is the force constant for two angle terms (IJK and IJL) sharing a common central bond (IJ) and a common central atom (J).

(vi) Two-center angle–angle terms

$$E_{2aa} = F\cos\phi(\cos\theta_{IJK} - \cos\theta_{aIJK})(\cos\theta_{JKL} - \cos\theta_{aJKL}) \tag{9}$$

where $k_{2\theta\theta} = F\cos\phi\sin\theta_{aIJK}\sin\theta_{aJKL}$ is the force constant for angle terms (IJK and JKL) in which the central atoms (J and K) are bonded to each other.

These cross terms are considered collectively as

$$E_x = E_{ax} + E_{1aa} + E_{2aa} \tag{10}$$

B. Nonbond Interactions. The electrostatic part (E_Q) of the nonbond interaction (3) is described by using the Coulomb expression

$$E_Q = \frac{Q_I Q_J}{\epsilon_0 \epsilon R_{IJ}} \tag{11}$$

where Q_I is the charge on center I (electron units), $\epsilon = 1$, and the constant $1/\epsilon_0 = 332.0637$ gives E in kcal/mol when R_{IJ} is the distance in Å.

Experimental and theoretical studies on alkanes suggest that all hydrogens have about the same charge. Thus, Hartree–Fock (HF) calculations[1] [all with the same valence double zeta basis with polarization functions on C and H] lead to Mulliken populations of $Q_H = 0.118$ for CH_4, $Q_H = 0.111$ for C_2H_6, $Q_H = 0.109$ and 0.108 for the terminal and central groups of propane, and $Q_H = 0.108$ and 0.106 for the terminal and central groups of n-butane. In comparison, fitting point charges to match electrostatic potentials from HF calculations (with similar basis sets) for CH_4 leads to Q_H of 0.124[2b] and 0.139,[2a] while the calculated octupole moment of methane using a high-quality CI wave function[3] yields $Q_H = 0.150$. On the basis of these results, we used

$$Q_H = 0.144|e|$$

in all calculations for polyethylene and n-butane. (The charges of carbon atoms are taken as $-0.144|e|$ times the number of bonded hydrogen atoms.)

The vdW part of the nonbond interaction (3) for atoms I and J is described by using the exponential-6 potential

$$E_{vdW_{IJ}} = Ae^{-BR_{IJ}} - \frac{C}{R_{IJ}^6} = \frac{D_v}{(\zeta - 6)}[6e^{\zeta(1-\rho)} - \zeta\rho^{-6}] \tag{12}$$

where $\rho = R_{IJ}/R_v$. These parameters are obtained empirically as described below.

C. The Hessian-Biased Force Field. The valence force field parameters for polyethylene (PE) are obtained by using the Hessian-biased method[4] for the valence force field of n-butane

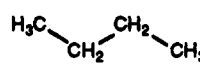

(13)

where the parameters associated with the central CH_2 units apply to PE. In the Hessian-biased approach, we input two quantities: (a) the experimental frequencies ν_i^{exp} of the $3N - 6$ normal modes of n-butane,[5] and (b) the analytical second derivative matrix or Hessian,

$$B_{\alpha I,\beta J}^{HF} = \frac{\partial^2 E^{HF}}{\partial X_{\alpha I}\,\partial X_{\beta J}} \tag{14}$$

(where $\alpha, \beta = x, y, z$ and $I, J = 1, 2, ..., N$, for an N-atom system), from the HF wave function of n-butane.

Defining the mass-weighted Hessian from the HF wave functions

$$\bar{B}_{\alpha I,\beta J}^{HF} = B_{\alpha I,\beta J}^{HF}/[M_I M_J]^{1/2} \tag{15}$$

the vibrational eigenfunctions are obtained from the eigenvalue equation

$$\bar{\mathbf{B}}^{HF}\mathbf{U}_i^{HF} = \mathbf{U}_i^{HF}\lambda_i^{HF}, \qquad i = 1, ..., 3N \tag{16}$$

The eigenvalues λ_i^{HF} are related to the vibrational frequencies ν_i^{HF}

$$\lambda_i = \kappa(\nu_i^{HF})^2 \tag{17}$$

(where $\kappa = 8.48027 \times 10^{-5}$ if masses are in atomic mass units, energies are in kcal/mol, distances are in Å, and ν_i are in cm^{-1}). However, the ν_i^{HF} differ by up to 20% from experiment, ν_i^{exp}.

(1) Dasgupta, S.; Goddard III, W. A. "Hessian-Biased Force Fields for Alkanes". To be submitted for publication.
(2) (a) Cox, S. R.; Williams, D. E. *J. Comput. Chem.* **1981**, *2*, 304. (b) Chirlian, L. E.; Francl, M. M. *J. Comput. Chem.* **1987**, *8*, 894.
(3) Amos, R. D. *Mol. Phys.* **1979**, *38*, 33. The charge was calculated by using a C–H bond length of 1.093 54 Å.
(4) Dasgupta, S.; Goddard III, W. A. *J. Chem. Phys.* **1989**, *90*, 7207.
(5) Cangeloni, M. L.; Schettino, V. *Mol. Cryst. Liq. Cryst.* **1975**, *31*, 219.

The B_{ij}^{HF} are used to specify the vibrational eigen*functions* and the ν_i^{exp} are used to determine the vibrational eigen*values*. Combining these leads to a new Hessian determined partly from experiment and partly from theory.

The Hessian-biased $\mathbf{B}^{BH}$ is defined as

$$B_{\alpha I,\beta J}^{BH} = [M_I M_J]^{1/2} \bar{B}_{\alpha I,\beta J}^{BH} \tag{18}$$

where

$$\bar{\mathbf{B}}^{BH} = \mathbf{U}^{HF} \lambda^{exp} \tilde{\mathbf{U}}^{HF} \tag{19}$$

λ^{exp} is the diagonal matrix with elements $\lambda_i^{exp} = \kappa(\nu_i^{exp})^2$, and $\tilde{\mathbf{U}}$ is the transpose of $\mathbf{U}$. Thus, by construction $\mathbf{B}^{BH}$ leads to the experimental vibrational frequencies and the theoretical vibrational eigenfunctions. We then determine the force field parameters for the terms (4)–(9) so that the force-field Hessian matches the biased Hessian

$$\frac{\partial^2 E^{FF}}{\partial X_{\alpha I}\, \partial X_{\beta J}} \approx B_{\alpha I,\beta J}^{BH} \tag{20}$$

[In these calculations (11) and (12) are included but the parameters Q_I, ζ, D_v, and R_v are kept fixed.] We also require that this force field lead to zero forces at the experimental geometry

$$\frac{\partial E^{FF}}{\partial X_{\alpha I}} \approx 0 \tag{21}$$

The result for *n*-butane is a total of

$$(3N-6)(3N-5)/2 + (3N-6) = 3(3N-6)(N-1)/2 = 702 \tag{22}$$

conditions, sufficient to determine the 76 parameters of even the most elaborate (MCXX) force field. To extract the force field parameters, we use a least-squares procedure in which the errors in satisfying (20) and (21) are simultaneously minimized.[1,4]

The HF calculations (including analytic second derivatives) were carried out with the GAUSSIAN-86 program.[6] The 6-31G** basis was used, which is valence double zeta on both C and H with d polarization functions on the C and p polarization functions on the H. These calculations were carried out at the experimental structure.[7]

D. Procedures for the Valence Force Field. We optimized the valence force field of *n*-butane using three levels of force field [all with electrostatic (11) and vdW (12) interactions]: (a) MC, Morse (4), cosine angle bend (5), torsion (6), electrostatic (11), vdW (12) but not cross terms; (b) MCX, MC plus bond-angle and bond–bond cross terms (7); (c) MCXX, MCX plus angle–angle cross terms (8), (9). These valence force fields (along with the force fields of methane, ethane, and propane) are discussed in more detail elsewhere.[1] The bond energy parameter (D_b) for the Morse potentials was fixed at a typical experimental value for the bond of interest and not optimized [the normal modes are not sensitive to D_b].

The notation on cross terms is illustrated as follows.

The angle cross terms (7) for the H–C–C angle involve two $k_{r\theta}$ terms denoted as $k_{H\theta}$ and $k_{C\theta}$ and one stretch–stretch term denoted k_{HC}.

For the tetrahedral center

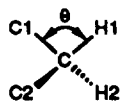

(23)

(6) Frisch, M. J.; Binkley, J. S.; Schlegel, H. B.; Raghavachari, K.; Melius, C. F.; Martin, R. L.; Stewart, J. J. P.; Bobrowicz, F. W.; Rohlfing, C. M.; Kahn, L. R.; Defrees, D. J.; Seeger, R.; Whiteside, R. A.; Fox, D. J.; Fleuder, E. M.; Pople, J. A. Carnegie-Mellon Quantum Chemistry Publishing Unit, Pittsburg, PA, 1984.

(7) No reliable μ-wave experimental structure is available for *n*-butane. The available electron diffraction studies [Bonham, R. A.; Bartell, L. S. *J. Am. Chem. Soc.* **1959**, *81*, 3491. Kuchitsu, K. *Bull. Chem. Soc. Jpn.* **1959**, *32*, 748] report average length and angle values for a 60:40 mixture of trans and gauche conformers. Consequently, for our ab initio calculations, we based the structure for *n*-butane on the microwave structure of propane (Lide, Jr., D. *J. Chem. Phys.* **1960**, *33*, 1514).

TABLE I: Valence Force Field Parameters Used in the Calculations for Polyethylene[a]

		n-butane		
		MCXX	MCX	MC
		Bond Stretch (Eq 4)		
C–C	R_b	1.4841	1.4720	1.5221
	k_b	884.9940	960.7682	570.0549
	D_b	(85.80)	(85.80)	(85.80)
C–H	R_b	1.0765	1.0702	1.0908
	k_b	741.3720	774.0032	672.4147
	D_b	(95.10)	(95.10)	(95.10)
		Angle Bend (Eq 5)		
H–C–H	k_θ	55.6076	46.0545	29.8261
	θ_a	119.3933	124.5427	134.0770
C–C–H	k_θ	65.7301	72.5454	67.8248
	θ_a	117.7291	119.7212	122.6576
C–C–C	k_θ	84.1810	76.0945	89.4018
	θ_a	121.2400	124.6770	123.5544
		Torsion (Eq 6)		
H–C–C–H	V_t	5.1686	3.5854	4.6266
C–C–C–H	V_t	6.1626	6.4680	6.8816
C–C–C–C	V_t	5.7070	6.3298	11.5449
		Angle Cross Terms (Eq 7)		
H–C–H	$D_{H\theta}$	−22.6583	−26.8877	
	k_{HH}	3.1321	3.2767	
C–C–H	$D_{C\theta}$	−34.3195	−36.9016	
	$D_{H\theta}$	−25.9234	−28.3688	
	k_{HC}	1.3684	1.4648	
C–C–C	$D_{C\theta}$	−54.0185	−55.0881	
	k_{CC}	26.2187	26.1288	
		One-Center Angle–Angle Cross Terms (Eqs 8 and 24)		
$G_{CC:HC}$		−7.6083		
$G_{CC:HH}$		−5.3356		
$G_{CH:CC}$		−5.0824		
$G_{CH:CH}$		−5.3356		
		Two-Center Angle–Angle Cross Terms (Eqs 9 and 26)		
$F_{H:CC:H}$		−17.7274		
$F_{C:CC:H}$		−16.4004		
$F_{C:CC:C}$		−21.5910		

[a] Units are kcal/mol for energies, Å for length, and degrees for angles. Values in parentheses were not optimized.

there are 12 one-center angle–angle terms of the form (8), each of which involves four atoms

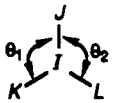

(24)

We denote the angle–angle force constant for (24) as $k_{IJ:KL}$ (where $k_{IJ:KL} = k_{IJ:LK}$). Thus, for PE there are four cases:

$$k_{CC:CH},\quad k_{CC:HH},\quad k_{CH:CC},\quad k_{CH:CH}$$

For a pair of adjacent centers, say, two carbons,

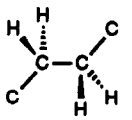

(25)

there is a total of $3^2 = 9$ two-center angle-angle terms, each of which involves four atoms

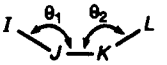

(26)

Here we denote the force constant as $k_{IJ:KL}$ (where $k_{LKJI} = k_{IJK:L}$). Thus, for PE there are three cases: $k_{C:CC:C}$, $k_{C:CC:H}$, and $k_{H:CC:H}$.

The valence FF parameters were optimized for *n*-butane (with the vdW parameter fixed) and then used (without readjustment) for polyethylene, whereas the vdW parameters were optimized for PE with fixed valence parameters (vide infra). As a result, we carried out a cycle of such optimizations. The final valence

TABLE II: van der Waals Parameters for C and H[a]

	LJ12-6[f]	exponential-6								exptl	Williams[h]
vdW parameters (eq 12)					OPT[i]			OPT[i]			
ζ_C		11.0	11.0	12.0	12.0	12.0	13.0	13.0	13.0		14.0340
R_{vC}, Å	3.8050	3.9425	3.9425	3.8837	3.8837	3.8837	3.8410	3.8410	3.8410		3.8983
D_{vC}, kcal/mol	0.06921	0.09115	0.09115	0.08444	0.08444	0.08444	0.07918	0.07918	0.07918		0.0951
ζ_H		12.0	13.0	11.0	11.8	12.0	11.0	11.2	12.0		12.3822
R_{vH}, Å	2.9267	3.3400	3.2212	3.2705	3.1975	3.1840	3.1810	3.1665	3.1132		3.3107
D_{vH}, kcal/mol	0.0335	0.00830	0.01144	0.0145	0.0160	0.01613	0.0199	0.0200	0.0210		0.0128
cohesive energy,[j] kcal/mol	1.838	1.849	1.860	1.849	1.857	1.852	1.863	1.851	1.829	1.838 ● 0.032[b]	1.686
zero-point energy cor,[j] kcal/mol	0.291	0.161	0.191	0.171	0.189	0.191	0.189	0.192	0.205		0.270
stress, GPa											
σ_{xx}	0.0033	−0.0940	−0.0670	−0.0853	−0.0655	−0.0619	−0.0689	−0.0649	−0.0501	0	−0.1473
σ_{yy}	−0.0029	0.0950	0.0679	0.0835	0.0672	0.0630	0.0646	0.0638	0.0512	0	−0.0587
setting angle, deg	41.7	42.4	42.3	42.4	42.3	42.4	42.4	42.4	42.3	41 ± 1[g]	43.4
lattice modes, cm^{-1}											
A_u	67	43	49	45	48	49	47	48	51		44
B_{3g}	87	67	74	73	74	75	78	78	78	(108[d])	104
B_{1u}	94	79	84	83	84	85	86	86	86	80[c]	97
B_{2u}	142	112	122	114	119	120	117	118	122	109[c]	125
A_g	198	126	147	129	141	144	137	140	150	137[d]	144
av error,[e] cm^{-1}	36.0	5.0	9.0	5.3	6.0	7.7	4.7	6.0	10.7		13.3
rms error,[e] cm^{-1}	40.8	6.6	9.7	5.7	6.6	8.1	5.8	6.5	11.2		14.1

[a] The calculations were carried out for the experimental structure at 4 K.[g] The optimum values are for $\zeta_H = 11.8$ with $\zeta_C = 12.0$ and $\zeta_H = 11.2$ with $\zeta_C = 13.0$. [b] Reference 14. [c] Reference 15. [d] Reference 16. See discussion in section VI.A about the B_{3g} mode. [e] Using B_{1u}, B_{2u}, and A_g modes. [f] $E_{LJ} = D_v[(R_v/R)^{12} - 2(R_v/R)^6]$. [g] Reference 13. [h] Reference 10. [i] These are the two sets of optimum parameters. We have selected $\zeta_C = 13.0$ for the other studies in this paper. [j] The calculated cohesive energy was corrected by subtracting the calculated zero-point-energy correction from using 1, 1, and 2 points in k_a, k_b, and k_c directions in the Brillouin zone.

FF parameters reported in Table I were optimized by using the $\zeta_H = 11.2$ and $\zeta_C = 13.0$ vdW parameters of Table II.

The final parameters are listed in Table I. The presence of cross terms leads to changes in the diagonal parameters as cross terms are added.

E. Procedure for the Nonbond Interactions. In a study of the elastic properties of graphite,[8] a force field for carbon was developed by requiring that the experimental parameters, elastic constants, and vibrational frequencies be reproduced. For the nonbond interactions, the available experimental data (c lattice parameter and C_{33} elastic constant) allowed two vdW parameters (R_{vC} and D_{vC}) to be specified for an exponential-6 potential (12) but not the third (ζ_C). As a result, a family of parameters were reported where $\zeta_C = 11$, 12, and 13 (see Table II). In the current paper we use the exponential-6 form (12) and optimize the vdW parameters for hydrogen (ζ_H, R_{vH}, D_{vH}) for each choice of ζ_C, as described below. For hydrogen–carbon interactions we assume the combination rules,

$$A_{HC} = (A_{HH}A_{CC})^{1/2}$$

$$B_{HC} = \tfrac{1}{2}(B_{HH} + B_{CC})$$

$$C_{HC} = (C_{HH}C_{CC})^{1/2}$$

These rules allow the accuracy-bounded convergence acceleration (ABCA) calculations to be optimized[9] and have been found adequate in previous studies.[10]

The most complete previous studies of vdW parameters for H and C is due to Williams and co-workers.[10] Considering the X-ray crystal structures of a number of hydrocarbons, Williams[10] estimated the charges, fixed the internal structure of each molecule (based on the X-ray studies), and optimized the C and H exponential-6 parameters to obtain the most accurate unit cell parameters and sublimation energies. For two molecules (n-hexane and benzene), there are accurate sublimation energies for 0 K and hence these molecules were emphasized. Since these data fixed only two parameters, Williams selected $\zeta_C = 14.034$ based on theoretical estimates.

Using our new vdW parameters for C, we initially optimized the H vdW parameters by fitting to n-hexane and benzene. However, a better procedure is to fit to the properties of PE. A major reason for this is that the crystal structure data for n-hexane[11] are available only at 160 K and for benzene[12] only at 77 K, whereas for optimization we need to compare with the crystal parameters near 0 K. On the other hand, there are structural parameters for PE down to 4 K.[13] In PE there are accurate experimental data[14] for the sublimation energies near 0 K. Data for the lattice-mode (vibrational) spectra in the crystal are available for all three systems, but for PE[15,16] these modes are accurately known near 0 K, whereas for n-hexane[17] and benzene[18] the experimental values are at higher temperatures (20 and 77 K, respectively).

At this point we would like to make a plea for accurate experimental studies of cell parameters, thermodynamics, elastic constants, and phonon dispersions of crystals at the lowest possible temperatures, (say 4 K). Such data are essential for determining the accurate vdW parameters needed for quantitative simulations of the properties of polymers, ceramics, and biological systems. With better data we could develop representations of the vdW potentials more accurately than exponential-6 and we could consider inclusion of the three-body terms that could be important at short range. Our perspective is that the technology has been available for such studies for over 20 years but that in the United States and many other countries, funding for such fundamental studies has lagged.

To determine the vdW parameters for H, we considered the polyethylene crystal and varied the vdW parameters (12) to obtain accurate cell parameters, lattice frequencies, and sublimation energies. These are the only experimental quantities sensitive to vdW interactions that are known near 0 K. Of the internal coordinates, the most relevant quantity is the setting angle, θ, which

(8) Goddard III, W. A.; Karasawa, N. "Elastic Constants and Phonon States for Graphite; van der Waals Parameters for Carbon". *J. Phys. Chem.*, submitted for publication.
(9) Karasawa, N.; Goddard III, W. A. *J. Phys. Chem.* **1989**, *93*, 7320.
(10) Williams, D. E.; Cox, S. R. *Acta Crystallogr.* **1984**, *90*, 404.
(11) Norman, N.; Mathisen, H. *Acta Chem. Scand.* **1961**, *15*, 1755.
(12) Bacon, G. E.; Curry, N. A.; Wilson, S. A. *Proc. R. Soc. London, Ser. A* **1964**, *279*, 98.
(13) Avitabile, G.; Napolitano, R.; Pirozzi, B.; Rouse, K. D.; Thomas, H. W.; Wills, B. T. M. *J. Polym. Sci., Polym. Lett. Ed.* **1975**, *13*, 351.
(14) Billmeyer, Jr., F. W. *J. Appl. Phys.* **1957**, *28*, 1114.
(15) Dean, G. D.; Martin, D. H. *Chem. Phys. Lett.* **1967**, *1*, 415.
(16) Harley, R. T.; Hayes, W.; Twisleton, J. F. *J. Phys. C* **1973**, *6*, L167.
(17) Brunel, L-C; Dows, D. A. *Spectrochim. Acta, Part A* **1974**, *30*, 929.
(18) (a) Sataty, Y. A.; Ron, A.; Brith, M. *Chem. Phys. Lett.* **1973**, *23*, 500. (b) Sataty, Y. A.; Ron, A. *J. Chem. Phys.* **1976**, *65*, 1578.

TABLE III: Comparison of Electrostatic Energy (E_Q) and van der Waals energy (E_v) of Polyethylene from (a) Accuracy-Bounded Convergence Acceleration (ABCA) Procedures and (b) Direct Summations[a]

(a) ABCA

ϵ_Q, kcal/mol	E_Q, kcal/mol	R_Q, Å	H_Q, Å^{-1}	η_Q, Å	ϵ_v, kcal/mol	E_v, kcal/mol	R_d, Å	H_d, Å^{-1}	η_d, Å	R_r, Å	N_{real}	N_{rec}
0.05	0.1351	4.1	4.3	1.7	0.01	−5.5729	5.1	4.2	1.8	5.6	560	189
0.005	0.1299	4.7	4.7	1.6	0.001	−5.5749	5.7	4.6	1.8	6.4	832	231
0.0005	0.1313	5.4	5.0	1.6	0.0001	−5.5747	6.1	5.1	1.7	7.2	1244	585

(b) Direct Sum

R_{cut},[b] Å	E_Q, kcal/mol	E_v, kcal/mol	N_{real}
9	−69.4635	−4.6865	2388
15	26.7702	−5.4015	11308
25	−31.8484	−5.5386	52743
35	12.8783	−5.5618	144895

[a] Here ϵ is the specified accuracy parameter. Cutoff distances in real space (R) and reciprocal space (H), convergence parameters (η), number of cells in reciprocal space (N_{rec}), and number of atom pairs used in real space (N_{real}) are shown for each ϵ. Subscripts are Q for electrostatic, d for dispersion, r for repulsive, and v for van der Waals (sum of dispersion and repulsion terms). [b] Using a cubic spline function to decrease the potential from full value at R_{cut} − 1 Å to zero at R_{cut}.

is the angle between the *ac* lattice plane and the CC plane of either chain. As indicated in Table II, the setting angle is independent of the vdW parameters, and we did not use the setting angle in fitting parameters. In these studies, we considered a range of values for ζ_H and used the experimental cell parameter and cohesive energies to determine the optimum R_{vH} and D_{vH} for each ζ_H. [We required that the residual stress in the *a* and *b* directions add to zero for the experimental cell parameters.]

We optimized all $3N = 36$ internal coordinates simultaneously with the six cell coordinates. This leads to the results in Table II where we see that better fits of cell parameters are obtained for larger ζ_H. On the other hand, lattice frequencies are too large for large ζ_H. To obtain an exact fit we need a form of the vdW potential with a less repulsive inner wall than exponential-6. However, we do not believe there is enough data to test a more flexible function. We chose two sets, $\zeta_C = 13.0$, $\zeta_H = 11.2$ and $\zeta_C = 12$, $\zeta_H = 11.8$, as the best compromises. These values lead to a good description of the lattice frequencies and less than 1.5% error in the *a* and *b* lattice parameters. As shown in the table, these two sets give very similar results. In this paper, we use $\zeta_C = 13$ and $\zeta_H = 11.2$ for all the calculations (including optimization of valence parameters) for polyethylene. In addition to the properties of PE reported here, these vdW parameters were used to calculate various properties for a number of hydrocarbon crystals, leading to excellent results.[19]

In Table II we have also included the results using the van der Waals parameters of Williams.[10] These calculations use $\zeta_C = 14.0340$, $R_{vC} = 3.8983$, and $D_{vC} = 0.0951$; $\zeta_H = 12.3822$, $R_{vH} = 3.3107$, and $D_{vH} = 0.0128$. In the Williams approach the nonbond interactions are calculated with each CH bond shortened by 0.07 Å from the experimental value (from 1.096 to 1.026 Å for PE). In PE the charges are 0.102 on each H and −0.204 on each C.

We see that the cohesive energy is about 8% smaller than experiment. Also σ_{xx} and σ_{yy} are both negative, indicating that the optimum cell parameters would be too large for these parameters. This would be expected because Williams' parameters are fitted to room temperature lattice parameters. The average error for the lattice frequencies is 13.3 cm^{-1}, which is about twice as large as the errors for the parameters developed here.

III. Calculational Details

A. Nonbond Summations. For all calculations on crystals, we use the ABCA procedure[9] to optimize convergence of the Coulomb ($1/R$) and dispersion ($1/R^6$) energies. In ABCA the input data are the required accuracy in the energy (we generally use $\epsilon_Q = 0.005$ kcal/mol for electrostatic sums and $\epsilon_v = 0.001$ kcal/mol for vdW sums) rather than cutoff distances. The program then chooses Ewald parameters[9] η_Q and η_v for the electrostatic and dispersion sums and chooses cutoff distances R_{cut} and H_{cut} for the real space sums and reciprocal space sums so that the terms beyond the cutoffs sum to less than ϵ. This estimate of the error is obtained by converting the sum of terms past the cutoff (R_{cut} or H_{cut}) to an integral, leading to an analytic approximation to the total error.[9] For a wide range of Ewald parameters η one can find values of R_{cut} and H_{cut} that yield the desired accuracy ϵ; however, the number of terms required in the real space sum relative to the number for the reciprocal space sum increases with η. Since the computational costs for real space terms are a factor of 5 or 10 larger than for the reciprocal space sums, ABCA selects η so as to minimize computation cost while ensuring a given accuracy ϵ. Similarly for the repulsive (exponential) part of the vdW interactions, ABCA estimates the R_{cut} to achieve the specified accuracy ϵ_v. For the calculations of energies, forces, stresses, and second derivatives in this paper, we use $\epsilon_Q = 0.005$ kcal/mol and $\epsilon_v = 0.001$ kcal/mol. For purposes of predicting structure and unit cell parameters accuracies of 0.1 kcal/mol would be satisfactory.

The ABCA procedure is illustrated in Table III for PE. Here we see that changing the accuracy parameter for Coulomb sums from $\epsilon_Q = 0.05$ to 0.005 to 0.0005 kcal/mol leads to $E_Q = 0.1351$, 0.1299, 0.1313 kcal/mol, consistent with the specified accuracies. This requires real space sums out to 4.1, 4.7, and 5.4 Å, respectively, and 560, 832, and 1244 pairwise interactions. [Actually fewer terms are required; the N_{real} in Table III is determined by the largest R_{cut} (which is R_r in each case) and the program evaluates E_Q using the smaller set satisfying R_Q.] In contrast, the direct sum approach using cutoffs of 9, 15, 25, and 35 Å leads to energies of −69.46, 26.77, −31.85, and +12.88 kcal/mol, respectively, with 2388, 11 308, 52 743, and 144 895 pairwise interactions. Thus it would be far more accurate to ignore charges than to evaluate E_Q with the direct summation approach! For the dispersion energy the errors in the direct approach are smaller but still too large (16% error for 9 Å cutoff, 3% error for 15 Å cutoff) for accurate properties.

B. Optimization. All calculations were carried out using POLYGRAF,[20] an interactive molecular simulations package for molecular mechanics and molecular dynamics of polymer crystals. During the calculations, the $3N = 36$ atomic coordinates and the six cell coordinates were simultaneously optimized and displayed on an Evans & Sutherland PS330 graphics system at each optimization cycle. The atomic coordinates were optimized by using conjugate gradient techniques until the rms force per degree of freedom became less than 0.02 (kcal/mol)/Å. All six cell parameters were also optimized by using conjugate gradient techniques (where the internal coordinates were optimized for each

(19) Karasawa, N.; Goddard, W. A. "Lattice Properties and van der Waals Parameters for Hydrocarbons". To be submitted for publication.

(20) POLYGRAF is an interactive molecular simulation/three-dimensional graphics program from Molecular Simulations Incorporated, Pasadena, CA 91101.

TABLE IV: Optimized Cell Parameters and Setting Angle (θ) of Polyethylene Crystal Using *n*-Butane Parameter Sets[a]

	a	b	c	α	β	γ	θ
n-butane MC	7.202	4.795	2.542	90.0	90.0	90.0	41.9
n-butane MCX	7.203	4.797	2.545	90.0	90.0	90.0	41.9
n-butane-MCXX	7.202	4.795	2.546	90.0	90.0	90.0	41.9
expt at 4 K[b]	7.121	4.851	2.548	90.0	90.0	90.0	41 (1)

[a] a, b, and c are in Å, and α, β, γ, and θ are in degrees (using ζ_C = 13.0 and ζ_H = 11.2). The setting angle is the angle between the ac plane and the plane containing the C–C bonds of a chain. [b] Reference 13.

choice of cell parameters) until the rms strain derivatives became less than 0.002 kcal/mol. At the optimized structure, all stress components are less than 0.0005 GPa.

C. Phonon States, Moduli, and Thermodynamics. Using the predicted equilibrium structure, we calculated the elastic constants and phonon frequencies from analytic first and second derivatives of the energy. These elastic constants were used to calculate the Young's moduli (E_i) and compressibility (β).

Phonon frequencies for all 36 vibrational bands were calculated as a function of wavevector. We report the phonon dispersion in the [0 0 1], [1 0 0], and [1 1 0] directions for PE crystal. In order to compare with neutron scattering data,[21] we also report the lattice modes in the [1 0 0] and [1 1 0] directions for deuteriopolyethylene crystal.

To obtain thermodynamic properties we calculated all 36 phonon states for the 1000 equally spaced points in the Brillouin zone obtained by using 10 points along each reciprocal lattice vector. The quantum partition function of the crystal was then described in terms of the sum (properly weighted) of 36 000 Einstein oscillators (using the harmonic oscillator quantum partition function).

D. Finite Strains. The above properties relate to the equilibrium configuration of the PE crystal. In addition, we examined the response of this crystal to large strain (tension and compression) in the directions perpendicular to the chain axis. Sufficiently large strain in these directions fractures the crystal and creates a new surface. To simulate this behavior, we considered the calculational unit cell to contain four crystallographic unit cells in either the a or b directions and deformed the cell in the a or b directions, respectively. The procedure was first to strain the cell coordinates *without* changing the internal atomic coordinates (within each cell) and then reoptimize the internal coordinates while keeping the strain fixed. These studies used ABCA accuracy parameters of ϵ_q = 0.005 kcal/mol and ϵ_v = 0.001 kcal/mol. Optimization of atomic coordinates continued until rms forces were less than 0.05 (kcal/mol)/Å.

These calculations were carried out with two boundary conditions for the cell coordinates perpendicular to the strain direction:

(a) zero stress—the cell coordinates perpendicular to the strain are optimized along with the atomic coordinates to obtain zero stress;

(b) fixed strain—the cell coordinates perpendicular to the strain are kept fixed at the unstrained values. Case a simulates the conditions of a real experiment where the crystal would relax to obtain zero stress perpendicular to the applied stress.

IV. Structure and Cohesive Energy

A. Crystal Structures. The optimized structures of PE are shown in Table IV along with the experimental values.[13] With full optimization of cell parameters and atomic coordinates, the cell angles are all 90 ± 0.1°. For the chain direction (c) the calculated cell parameter (*n*-butane MCXX) is 0.08% smaller than experiment (at 4 K). The differences in c for various force fields seem to arise from very small shifts in the equilibrium C–C bond distance. For the directions (a, b) perpendicular to the chains the errors are 1.1% for a and −1.1% for b (*n*-butane MCXX). These parameters depend mainly on the vdW parameters, which are unchanged. Perhaps the changes in b are due to small changes in the equilibrium C–C–C angle. The calculated setting angle is θ = 41.9°, which agrees quite well with the experimental value of 41 ± 1° at 4 K.

TABLE V: Geometries and Properties of Isolated Chain and Chain of Optimum Crystal

	isolated chain	chain of optimum crystal
lattice parameters, Å		
c	2.5459	2.5457
bond distances, Å		
C–C	1.533	1.532
C–H	1.096	1.095
bond angles, deg		
C–C–C	112.30	112.42
H–C–H	108.81	108.64
C–C–H	108.92	108.93
velocity of sound		
v_c, km/s	17.8	17.9
Young's modulus		
E_c, GPa	335.7	337.1

TABLE VI: Theoretical and Experimental Lattice Energy of Polyethylene Crystal[a]

	total energy	zero-point energy	lattice energy[c]
isolated chain	3.9035	17.4199	
crystal	1.8549	17.5984	
difference	2.0486	−0.1785	1.8701
experiment			1.838 ● 0.032[b]

[a] All energies in kcal/mol per CH_2. [b] Reference 14. [c] Total energy corrected for zero-point energy.

B. Lattice Energy. Using all available thermodynamic data (heats of fusion, heats of vaporization, and heat capacities) on *n*-alkanes, Billmeyer[14] estimated the cohesive energy of crystalline PE at 0 K as

$$\Delta H_{0K}^{subl} = 1.838 \pm 0.032 \text{ kcal/mol}$$

per CH_2 group. This is the energy to separate the PE crystal into isolated all-trans PE chains.

To calculate the energy and zero-point energy of the isolated chain, we used a single chain in the three-dimensional tetragonal cell with $a = b$ = 100 Å and optimized the atomic coordinates and cell parameters. a and b do not change during the optimization, indicating that the chains can be regarded as isolated. In Table V we see that there are small changes in the structural parameters when the lateral forces of the crystal are absent. Thus the C–C–C bond angle increases by 0.12°, while the H–C–H angle decreases by 0.17°. Also the CH and CC bond distances decrease by 0.001 Å.

At the optimized structure, the zero-point energy is calculated by using 1000 points in Brillouin zone. As indicated in Table VI, the lattice energy per CH_2 group is calculated as 2.0486 kcal/mol (*n*-butane force field). After the zero-point energy is corrected, this value becomes 1.8701 kcal/mol, which can be compared with the experimental value[14] of 1.838 ± 0.032 kcal/mol at 0 K.

V. Moduli and Elastic Constants

A. Young's Modulus. Although it is not yet possible to obtain single crystals of PE, it is possible (by successive drawing along the chain axis) to obtain fibers in which the crystalline regions are highly oriented, with the chain axis along the fiber axis. Thus there are a number of experimental measurements for the Young's modulus *along* the chain direction, E_c. Unfortunately, careful experimental results span the range from 210 to 340 GPa!

1. Review of Experiments on Young's Modulus. Using X-ray diffraction to observe directly the changes in cell coordinates for various crystallites as stress is applied leads to a Young's modulus (at room temperature) of 235 GPa[22] or 213–229 GPa.[23] Since

(21) Twisleton, J. F.; White, J. W.; Reynolds, P. A. *Polymer* **1982**, *23*, 578.

(22) Sakurada, I.; Nukushina, Y.; Ito, T. *J. Polym. Sci.* **1962**, *57*, 651.
(23) Matsuo, M.; Sawatari, C. *Macromolecules* **1986**, *19*, 2036.

TABLE VII: (a) Comparison between Elastic Constants Using Various Force Fields at Optimized Cell Parameters. (b) Elastic Constants from Various Experimental Cell Parameters Using *n*-Butane MCXX Force Field Parameters[a]

(a)

	n-butane		
	MCXX	MCX	MC
C_{11}	14.0	14.0	13.9
C_{22}	13.5	13.6	13.5
C_{33}	338.9	287.1	237.9
C_{12}	7.9	7.9	7.9
C_{13}	2.1	2.8	2.3
C_{23}	4.8	5.4	4.8
C_{44}	5.3	5.4	5.4
C_{55}	3.0	3.0	3.0
C_{66}	5.9	6.0	5.9
E_a	9.4	9.4	9.3
E_b	9.0	9.1	9.0
E_c	337.1	284.9	236.1
β, GPa^{-1}	0.0937	0.0936	0.0943
E_c (isolated chain)	335.7	283.2	234.4

(b)

	4 K[b]	77 K[c]	213 K[c]	303 K[c]	411 K[c]
C_{11}	14.9	13.3	10.6	8.3	3.9
C_{22}	12.9	11.2	9.6	8.2	5.4
C_{33}	338.2	333.2	325.7	318.4	306.5
C_{12}	7.8	6.9	5.4	4.3	3.7
C_{13}	2.2	1.8	1.2	0.7	0.09
C_{23}	4.2	3.5	3.0	2.5	1.9
C_{44}	4.8	4.0	3.5	3.0	2.5
C_{55}	2.9	2.5	2.1	1.7	1.4
C_{66}	6.7	6.1	4.7	3.6	2.3
E_a	10.2	9.1	7.5	6.1	1.3
E_b	8.8	7.6	6.8	6.0	1.8
E_c	336.8	332.1	324.7	317.6	304.6
β, GPa^{-1}	0.0945	0.107	0.130	0.161	0.258
a, Å	7.121	7.155	7.287	7.413	7.706
b, Å	4.851	4.899	4.918	4.942	4.936
c, Å	2.548	2.5473	2.5473	2.5473	2.5473
θ, deg	42.4	42.5	42.3	42.2	40.4

[a] All quantities in GPa unless otherwise indicated. [b] Cell parameters (a, b, and c) from ref 13. [c] Cell parameters (a, b, and c) from ref 31.

the crystallites are separated by amorphous regions, Matsuo and Sawatari[23] used samples with various draw ratios to determine the effects of amorphous regions in the crystal upon the measured Young's moduli and found no significant changes in E_c, indicating that $E_c \approx 225$ GPa is the intrinsic value (at 300 K) for the embedded crystallites.

An alternative strategy to oriented crystals is to grow PE fibers at 120 °C from solutions of high molecular weight PE in xylene.[24] With such fibers, Barham and Keller[25] used a dynamic tester to measure the tensile modulus and loss factor (tan δ) as a function of temperature. The direct measurement leads to a maximum modulus of $E_c = 262$ GPa (at 77 K), which they consider a lower bound. Correcting for finite strain rate and other factors, they estimate a true modulus at 77 K of $E_c = 288 \pm 10$ GPa, and they suggest that the modulus should increase to $E_c \approx 324$ GPa at 0 K.

This value of 288 GPa is the largest directly measured modulus for PE. Other estimates of the modulus come from spectroscopic studies or theory. Thus, using inelastic neutron scattering to measure the dispersion in the longitudinal acoustical phonon band of PE leads to $E_c = 329$ GPa[26] (from the slope of the dispersion curve) at 300 K.

An alternative estimate can be made by extrapolating the vibrational frequencies of accordion-like motions (from Raman spectroscopy) for the series of linear hydrocarbon molecules (C_{18} to C_{94}) to the value for an infinite chain.[27] One such extrapolation leads to a Young's modulus of 358 ± 25 GPa at 300 K for the infinite chain.[27] Another extrapolation includes corrections for the effect of interlamellar forces in the crystal and leads to an estimate fo 290 ± 5 GPa at 300 K for the infinite chain.[28]

TABLE VIII: Young's Moduli (in GPa) of Polyethylene[a]

	0 K	77 K	300 K
(a) E_c (chain axis)			
theory (MCXX, *n*-butane)	337	332	318
experimental			
direct			
X-ray			235[b]
X-ray			213–229[c]
dynamic tester	(324 ± 30)[g]	288 ± 10[f]	
spectroscopic			
neutron scattering			329[e]
Raman			358 ± 25[h]
Raman			290 ± 5[d]
(b) E_a (⊥ chain, long axis)			
theory (MCXX, *n*-butane)	9.4	9.1	6.1
experiment			
X-ray			3.2[i]
X-ray			2.5[i]
X-ray			5.0[i]
(c) E_b (⊥ chain, short axis)			
theory (MCXX, *n*-butane)	9.0	7.6	6.0
experiment			
X-ray			3.9[i]
X-ray			1.9[i]

[a] The theoretical values are calculated from $E_a = (S_{11})^{-1}$, $E_b = (S_{22})^{-1}$, $E_c = (S_{33})^{-1}$, where $\mathbf{S} = \mathbf{C}^{-1}$ is the compliance matrix. [b] Reference 22. [c] Reference 23. [d] Reference 28. Extrapolation from isolated *n*-alkane chains corrected for interlamellar interactions. [e] Reference 26. [f] Reference 25. [g] Estimated in ref 25. [h] Reference 27, extrapolation from isolated *n*-alkane chains. [i] Reference 29.

2. Calculations. The theoretical value of E_c depends strongly on the valence parameters of PE, most notably the angle–angle cross terms. Thus, with better fits to the force field of *n*-butane, we find more accurate values of E_c with $E_c = 236$ GPa for MC, 285 GPa for MCX, and 337 GPa for MCXX (see Table VII). Thus we take $E_c = 337$ GPa as the theoretical value, which is in agreement with the estimated value ($E_c \approx 324$ GPa at 0 K) from studies of high modulus PE on a dynamic tester. Various experimental results are tabulated in Table VIII.

Using the experimental cell parameters for 300 K, we calculate $E_c = 318$ GPa, which is in good agreement with the neutron scattering results of $E_c = 329$ GPa.

For the isolated chain (with the density at 300 K, 0.998 g/cm^3), we calculate $E_c = 316$ GPa, which is close to the average for the two extrapolations of Raman data (358 ± 25 GPa[27] and 290 ± 5 GPa[28]). Thus the interaction between chains leads to a 1.4 GPa increase (0.5%) in E_c (the correction is sensitive to the quality of the force field; see Table VIIa).

We carried out calculations of the vibrational frequencies for normal alkanes up to $C_{16}H_{34}$ using the MCXX force fields. The accordion modes from these calculations are compared with experiment in Table XIII where we see excellent agreement (about 0.7% lower than the least-squares fit[27] to data with higher N). In this table, we show the experimental frequencies observed in the liquid and solid phases[42] together with a least-squares fit to these frequencies.[27] This agreement suggests that our calculated elastic constants (318 GPa at 300 K and 337 GPa at 0 K) are about 1.4% lower than the true experimental values (suggested as 322 and 341 GPa, respectively).

Summarizing, the extrapolated modulus for the dynamic tester and the results from neutron scattering and Raman spectroscopy are all consistent with the theoretical values of Young's modulus, $E_c = 337$ GPa at 0 K and $E_c = 318$ GPa at 303 K. On the basis

(24) Zwitnewberg, A.; Pennings, A. J. *Colloid Polym.* **1976**, *252*, 868.
(25) Barham, P. J.; Keller, A. *J. Polym. Sci., Polym. Lett. Ed.* **1979**, *17*, 591.
(26) Holliday, L.; White, J. W. *Pure Applied Chem.* **1971**, *26*, 545, and references therein.
(27) Shaufele, R. F.; Shimanouchi, T. *J. Chem. Phys.* **1967**, *47*, 3605.
(28) Strobl, G. R.; Eckel, R. *J. Polym. Sci., Polym. Phys. Ed.* **1976**, *14*, 913.

TABLE IX: Comparison of Theoretical and Experimental Elastic Constants at 213 and 77 K[a]

	T = 213 K		T = 77 K	
	theory	exptl[b]	theory	exptl[c]
C_{11}	10.6	8.4	13.3	11.5
C_{22}	9.6		11.2	
C_{33}	325.7	102	333.2	
C_{12}	5.4	4.2	6.9	
C_{13}	1.2	5.5	1.8	
C_{23}	3.0		3.5	
C_{44}	3.5	1.81	4.0	
C_{55}	2.1		2.5	
C_{66}	4.7	2.02	6.1	
a	7.287		7.155	
b	4.918		4.899	
c	2.5473		2.5473	

[a] Cell parameters from ref 31 are used in the calculation. [b] Reference 30. The values for HDPE (draw ratio = 27) at −60 °C. [c] Reference 21.

of comparison to Raman data for linear alkanes, we estimate the exact results to be

$$E_c = 341 \pm 9 \text{ GPa} \quad \text{at 0 K}$$

$$E_c = 322 \pm 9 \text{ GPa} \quad \text{at 300 K}$$

In contrast, the Young's moduli in the a and b directions (perpendicular to the chain) depend most sensitively upon the vdW parameters and the temperature. We find E_a = 9.4 GPa and E_b = 9.0 GPa for the theoretical cell parameters and

$$E_a = 10.2 \text{ GPa} \quad \text{at 4 K}$$

$$E_b = 8.8 \text{ GPa} \quad \text{at 4 K}$$

for the experimental cell parameters at 4 K. This indicates that the interactions between the chains at the corner and center of the unit cell are stronger than those along the short (b) axis.

Experimental results for the moduli perpendicular to the chains (E_a and E_b) are expected to be far less reliable than for E_c because crystalline imperfections should greatly decrease the net bonding. In addition, thermal expansion leads to large decreases in those moduli as temperature is increased from 0 K to room temperature. Thus, using the experimental cell parameters at room temperature, we find

$$E_a = 6.1 \text{ GPa} \quad \text{at 300 K}$$

$$E_b = 6.0 \text{ GPa} \quad \text{at 300 K}$$

(decreases of 4.1 and 2.8 GPa, respectively). Three sets of experimental moduli perpendicular to the chain direction of PE have been reported:[29] (1) E_a = 3.2 GPa, E_b = 3.9 GPa, (2) E_a = 2.5 GPa, E_b = 1.9 GPa, and (3) E_a = 4.0 GPa. All are much smaller than the calculated moduli.

B. Elastic Constants. The calculated elastic constant values for various force fields are listed in Table VII. Only the chain–chain constant C_{33} changes appreciably, suggesting that for PE crystal the elastic constants involving distortions parallel to the chain are largely determined by the valence force field, while the perpendicular and shear elastic constants are largely determined by the nonbond force field.

Choy and Leung[30] measured the elastic constants of PE at 213 K using high-density polyethylene with a draw ratio of 27. This should orient the chains toward the axis, but incompletely. The result is a value of C_{33} = 102 GPa, which is less than one-third of the limiting value (326 GPa at 213 K). In Table IX we compare the experimental results with calculated values using the experimental unit cell at 213 K. The other experimental values are smaller than values obtained here except for C_{13} (see Table IX).

(29) Odajima, A.; Maeda, T. *J. Polym. Sci. C.* **1966**, *15*, 55.
(30) Choy, C. L.; Leung, W. P. *J. Polym. Sci., Polym. Phys. Ed.* **1985**, *23*, 1759.

TABLE X: Comparisons of Theoretical (MCXX) and Experimental Vibrational Frequencies (cm^{-1}) of Polyethylene Crystal at the Γ Point (Zone Center)

		calculations		
mode[b]	symmetry	optimum cell	(300 K)	expt[a] (300 K)
lattice	A_u	50	39	
	B_{3g}	82	65	(108)[d]
	B_{1u}	84	66	80[c]
	B_{2u}	115	88	109[c]
	A_g	132	105	137[d]
CH_2 rock	B_{2u}	784	783	720
	B_{1u}	798	791	731
	A_g	1164	1163	1168
	B_{3g}	1165	1164	1168
CH_2 twist	A_u	1031	1032	
	B_{3u}	1033	1033	1050
	B_{2g}	1306	1305	1295
	B_{1g}	1311	1308	1295
skeletal	B_{1g}	1046	1042	1061
	B_{2g}	1052	1046	1061
	B_{3g}	1101	1097	1131
	A_g	1101	1097	1131
CH_2 wag	A_u	1220	1219	
	B_{3u}	1216	1216	1175
	B_{1g}	1438	1435	1415
	B_{2g}	1441	1437	1415
CH_2 sciss	A_g	1461	1462	1440
	B_{3g}	1490	1485	1464
	B_{2u}	1484	1482	1463
	B_{1u}	1485	1481	1473
CH_2 sym str	B_{2u}	2873	2865	2851
	B_{1u}	2873	2868	2851
	B_{3g}	2890	2880	2848
	A_g	2892	2882	2848
CH_2 asym str	A_g	2924	2913	2883
	B_{3g}	2934	2922	2883
	B_{1u}	2937	2929	2919
	B_{2u}	2937	2929	2919
$\lvert\Delta\nu\rvert_{avg}$		24	24[e]	

[a] Reference 32 unless indicated otherwise. T = 300 K. [b] The modes are grouped by type and the label placed with the first mode of a type. [c] Reference 15. T = 2 K. [d] Reference 16. T = 4 K. [e] Excluding lattice modes.

There is also an experimental value of C_{11} = 11.5 GPa (at 77 K) from Twisleton et al.,[21] which can be compared with the calculated elastic constant of C_{11} = 13.3 GPa using cell parameters for 77 K[31] (see Table IX).

VI. Phonons and Thermodynamics

A. Vibrational Frequencies. The MCXX force field from *n*-butane leads to the vibrational levels of polyethylenes as reported in Table X (all at the Γ point or zone center). In these calculations, we did *not* change any parameters for *n*-butane; we used the predicted cell parameters and the experimental cell parameters at 300 K. The experimental vibrational frequencies of PE from infrared and Raman spectra are also listed in Table X (the lattice modes are for 2 and 4 K, but the higher modes are at 300 K). The average error for PE at room temperature is 24 cm^{-1}. In comparison, this force field leads to an average error of 7.9 cm^{-1} for the free molecule *n*-butane. Although we could have readjusted the valence force field to obtain a better fit to the vibrations, we have not done so here. The reason is that we consider this procedure of calculating the phonons and other properties of crystals using the valence force field for a finite molecule to be a prototype for similar calculations for many other polymers where experimental data are not available.

Overall agreement between calculated and experimental intramolecular frequencies is good. The exception occurs for the CH_2 rocking modes observed in PE at 720 and 731 cm^{-1} but

(31) Swan, P. R. *J. Polym. Sci.* **1962**, *56*, 403.
(32) Tasumi, M.; Shimanouchi, T. *J. Chem. Phys.* **1965**, *43*, 1245.

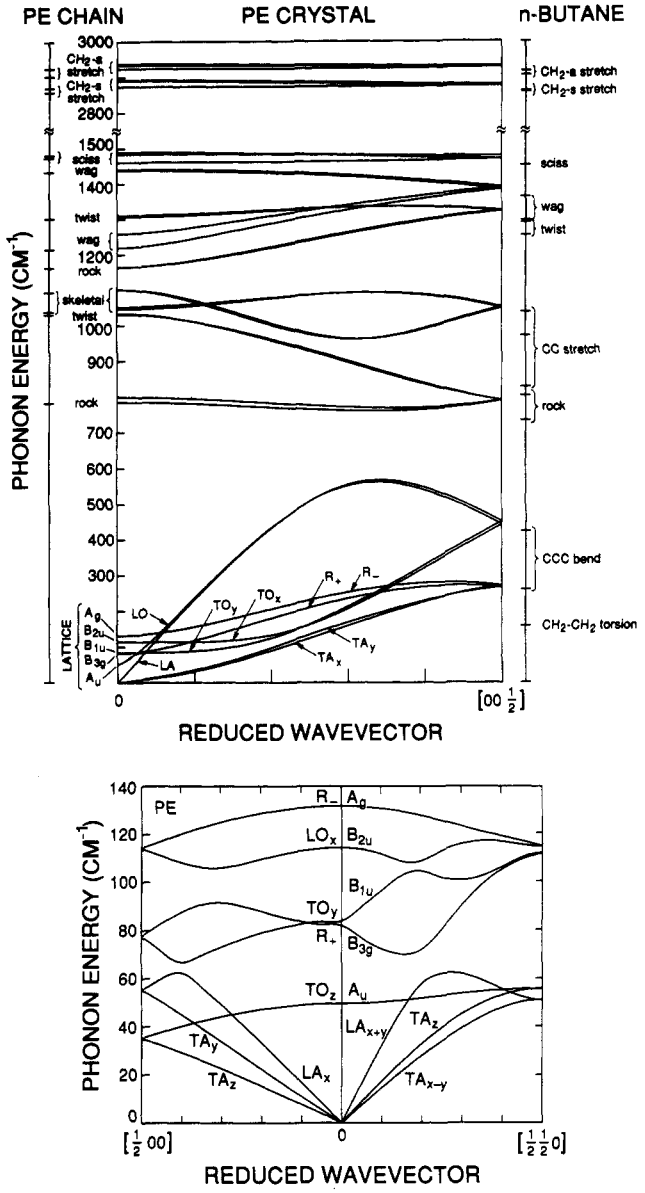

Figure 1. Phonon dispersion curves of polyethylene crystal (MCXX *n*-butane force field) (a, top) in the chain direction (*c* axis) and (b, bottom) in the [1 0 0] and [1 1 0] directions. In (a), frequencies of the isolated infinite chain at $k = 0$ and those of *n*-butane are also shown.

calculated at 789 and 798 cm^{-1}, respectively. The analogous mode for *n*-butane is well described (0.5 cm^{-1} error, observed at 733 cm^{-1}) where it involves a mixture of CH_3 rock and CH_2–CH_3 torsion modes. In contrast for PE, this mode corresponds to nearly pure CH_2 rock motion. Probably fitting to the modes of *n*-pentane or *n*-hexane (which have purer rock character) would have improved the comparison for PE. The temperature dependence of the splitting in the 720 and 731 cm^{-1} modes indicates that intermolecular interactions may also play some role in these modes.

In the case of B_u modes, we find that the frequency of the internal mode depends on the direction of the wave vector near the Γ point. In such modes, nonzero polarization is produced in the unit cell and a depolarization field is created. This field depends on the direction of the wave vector and affects the lattice distortion differently;[33] hence, the frequency depends on the direction of the wave vector. For example, the calculated frequency for the B_{2u} rocking mode is 784, 784, and 797 cm^{-1} for wave vectors in the *z*, *x*, and *y* directions, respectively. However, in this case, the allowed transition occurs only for the *z* and *x* directions, so that 784 cm^{-1} is quoted. Similarly for all other B_u

(33) Brüesch, P. *Phonons: Theory and Experiments I*; Springer-Verlag: Berlin, 1982.

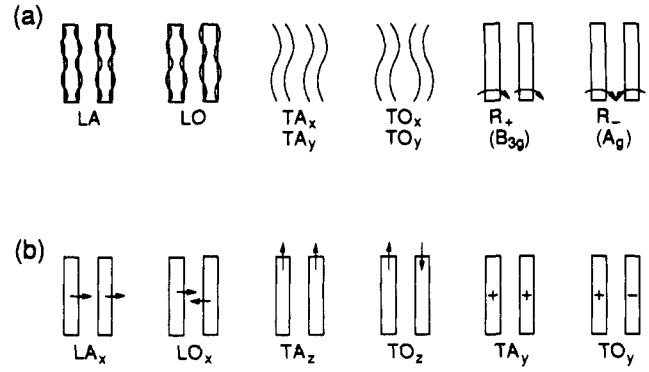

Figure 2. Schematic diagram for lattice modes of PE: (a) wave vector along chain axis; (b) wave vector perpendicular to chain axis.

modes, the allowed directions for the wave vector lead to equivalent results and only such values are quoted in Table X.

The various Raman and infrared (IR) experiments provide data for four of the five possible lattice modes. Three modes (B_{1u}, B_{2u}, and A_g) are strong and well resolved experimentally;[15,16] however, one mode, B_{3g}, is rather weak and observed at a value nearly concident with the B_{2u} mode.[16] Consequently, we used the three former states to select the optimum scale parameter ζ_H.

B. Phonon Bands. The phonon frequencies of the lattice bands calculated along the [0 0 1], [1 0 0], and [1 1 0] directions are shown in Figure 1.

Also indicated at the left in Figure 1 are the modes for the isolated chain (for the Γ point). Thus, the packing of PE fibers leads to only small changes in the positions of these levels. Also indicated at the left in Figure 1 are the positions of the vibrations in *n*-butane associated with the central CH_2 groups. From these comparisons we see that the modes associated with CH_2 motion in *n*-butane correspond closely to the modes in PE. In addition, the C–C stretch modes of *n*-butane correspond to the skeletal modes of PE. However, the C–C–C angle-bend and torsion modes of *n*-butane become lattice modes in PE.

The lattice modes can be understood by considering the crystal of PE fiber to be a collection of round rods packed together. This is indicated in Figure 2 for vibrations parallel and perpendicular to the chain direction. The energies of these lattice modes are sensitively dependent upon the vdW interactions. Indeed, we used the comparison with experiment to help determine the ζ_H vdW parameter. For the [0 0 $^1/_2$] point we see that the eight lattice modes have coalesced into four, at 268, 272, 442, and 451 cm^{-1}. These values correspond roughly to the g and u modes for C–C–C bend in *n*-butane (425 and 267 cm^{-1}, respectively). The torsion mode for the central bond in *n*-butane is at 155 cm^{-1}.

For wave vectors perpendicular to the chain (Figure 1b), the highest energy lattice mode is at 130 cm^{-1}. Thus, for temperatures above ~200 K, all such lattice modes are activated, allowing the spacing and orientations of the rods freedom to change rapidly. It is interesting that the glass transition temperature of PE is ~213 K, which corresponds reasonably well to the highest lattice mode perpendicular to the chain. This is reasonable since multiple energy loss processes for macroscopic deformation of the polymer become possible when all lattice modes are active. It will be interesting to see if the lattice modes of other polymers correlate with the glass temperature.

Inelastic neutron scattering experiments have been reported for deuteriopolyethylene in the direction [1 0 0] and [1 1 0],[21] and hence we calculated (Figure 3) the phonon bands of deuteriopolyethylene (using the experimental cell parameters at 77 K). For the [$^1/_2$ $^1/_2$ 0] direction there is excellent agreement in the dispersion for the lowest three observed transitions. The highest observed case lies in between the two calculated curves (LA_{x+y} and TO_z). Similarly for [$^1/_2$ 0 0], the lower energy transition corresponds well to LA_z, but the highest observed transition is between LA_x and TA_y.

Low-frequency Raman-active vibrations of *n*-paraffins have been studied by Wu and Nicol,[41] Olf and Fanconi,[39] and Vergoten

TABLE XI: Calculated Thermodynamic Properties of Polyethylene Crystal[a]

T, K	C_p, cal/(mol K)	C_v, cal/(mol K)	S, cal/(mol K)	U, kcal/mol	F, kcal/mol	$10^4\alpha$, K^{-1}	V, Å^3	β, GPa^{-1}
20	0.1769	0.1756	0.0689	0.0010	−0.0004	0.433	22.006	0.0946
40	0.6583	0.6473	0.3286	0.0091	−0.0041	0.907	22.036	0.0956
60	1.1836	1.1495	0.6869	0.0270	−0.0142	1.32	22.086	0.0975
80	1.6701	1.5990	1.0809	0.0546	−0.0318	1.67	22.151	0.1000
100	2.0944	1.9764	1.4795	0.0905	−0.0574	1.95	22.230	0.1031
120	2.4629	2.2931	1.8686	0.1333	−0.0909	2.17	22.324	0.1069
140	2.7875	2.5692	2.2432	0.1820	−0.1321	2.32	22.426	0.1114
160	3.0838	2.8240	2.6030	0.2360	−0.1805	2.41	22.530	0.1160
180	3.3583	3.0727	2.9500	0.2949	−0.2361	2.43	22.643	0.1213
200	3.6158	3.3258	3.2868	0.3589	−0.2985	2.37	22.749	0.1267
220	3.9075	3.5898	3.6160	0.4280	−0.3675	2.41	22.859	0.1325
240	4.2043	3.8677	3.9402	0.5025	−0.4431	2.43	22.970	0.1387
260	4.5141	4.1597	4.2612	0.5828	−0.5251	2.44	23.082	0.1450
280	4.8410	4.4646	4.5806	0.6691	−0.6135	2.48	23.195	0.1524
300	5.1937	4.7798	4.8993	0.7615	−0.7083	2.57	23.312	0.1601
320	5.5796	5.1022	5.2180	0.8603	−0.8095	2.73	23.436	0.1686
340	6.0067	5.4287	5.5372	0.9656	−0.9171	3.00	23.570	0.1790
360	6.4897	5.7565	5.8567	1.0774	−1.0310	3.38	23.720	0.1916
380	7.0399	6.0829	6.1767	1.1958	−1.1513	3.91	23.893	0.2086
400	7.6699	6.4059	6.4970	1.3207	−1.2780	4.59	24.096	0.2316

[a] The vibrational specific heat (C_p, C_v), entropy (S), energy (U), and free energy (F) are each per CH_2 of polyethylene crystal (using n-butane MCXX force parameters). Thermal expansion coefficient (α), volume (V), and compressibility (β), used to convert C_v to C_p, are also shown.

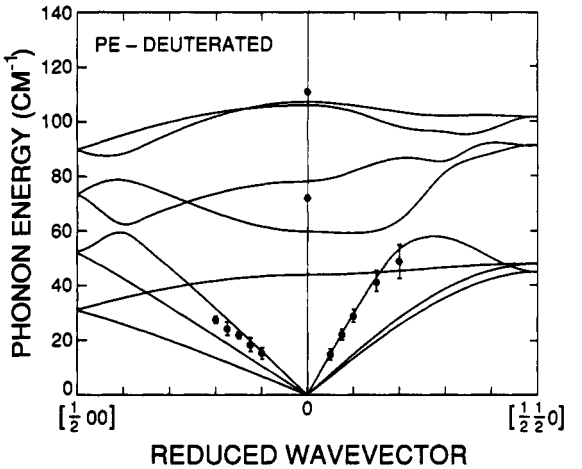

Figure 3. Phonon dispersion curves of deuteriopolyethylene crystal (MCXX n-butane force field) in the [1 0 0] and [1 1 0] directions. Experimental points are from ref 21.

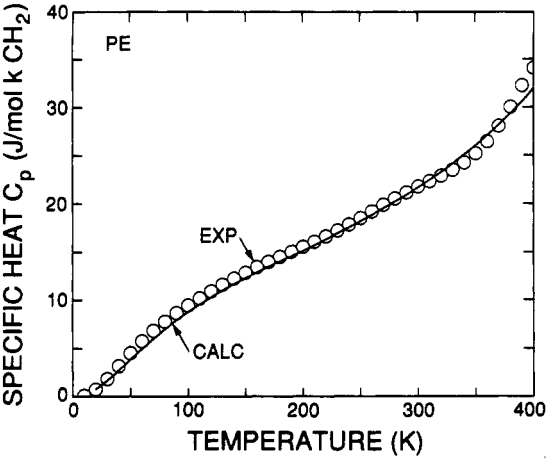

Figure 4. Calculated C_p and experimental[34] C_p versus temperature.

et al.[40] Olf and Fanconi[39] and Vergoten et al.[40] find that low-frequency modes of orthorhombic n-paraffins correspond to the transverse acoustical branches of polyethylene (TA_x and TA_y in Figure 1a). In Figure 8 we show these phonon bands calculated using the experimental cell parameters at 77 and 168 K (atomic coordinates and setting angles were optimized). As indicated in Figure 8, the modes assigned by Vergoten et al.[40] agree quite well with our calculations. However, the assignments by Olf and Fanconi do not agree with our calculations or with the results by Vergoten. Since our calculated bands perpendicular to the chain direction also agree well with the neutron-scattering experiments (which provide a more direct test), we suggest that the assignments for the experiments by Olf and Fanconi be reconsidered.

C. Thermodynamic Properties. Thermodynamic properties were calculated by using the phonon states at 0 K (see section III.C for details) and are reported in Table XI as a function of temperature.

The calculated values of specific heat at constant volume C_v were converted to constant pressure, C_p, using the thermodynamic relation $C_p = C_v + V\alpha^2T/\beta$, where V is the volume, α is the thermal expansion coefficient, and β is the compressibility [$\beta = \sum_{ij=1}^{3}(C^{-1})_{ij}$]. Temperature variations of cell parameters were measured by Swan[31] between 203 and 403 K. Experimental results are also available at 4 and 90 K.[13] Using spline fits to these data yields the $V(T)$ and $\alpha(T)$ in Table XI. With these cell parameters we calculated $\beta(T)$ as in Table XI. This leads to the $C_p(T)$ given in Table XI, and these are compared with experimental[34] $C_p(T)$ in Figure 4.

These calculations of the thermodynamic properties assume each normal mode (phonon) is harmonic, an approximation that becomes poorer at higher temperatures. This should underestimate C_v at high temperature. We see that the theoretical and experimental C_p are in excellent agreement below 300 K but diverge increasingly as the melting temperature (414.6 ± 0.5 K[34]) is approached.

VII. Finite Stress–Strain Relations

A. Stress and Ultimate Yield Stress. In Figure 5a, stresses are plotted as functions of deformation of the cell in the a and b directions. Here the cell parameters perpendicular to the deformation direction and the atomic coordinates are optimized starting from the structures optimized at fixed cell parameters. In both directions, there is a near singularity at a value (σ_{ult}) beyond which two new surfaces are created. Below this distance, the polymer rods are uniformly spaced. As the crystal is stretched, the rods separate further until a distance is reached at which it is better to create a surface and let all other chains relax to their normal distance. For the a direction, the yield point is σ_y = 0.097 GPa at 1.0% strain and the ultimate stress is σ_{ult} = 0.20 GPa at 3.5% strain. For the b direction we find ϵ_y = 0.23 GPa at 3.1% strain and σ_{ult} = 0.44 GPa at 8.3% strain.

In Figure 5 we see that the stress–strain relation is approximately linear (elastic) up to the yield point (σ_y), and it bends over

(34) Gaur, U.; Wunderlich, B. *J. Phys. Chem. Ref. Data* **1981**, *10*, 119.

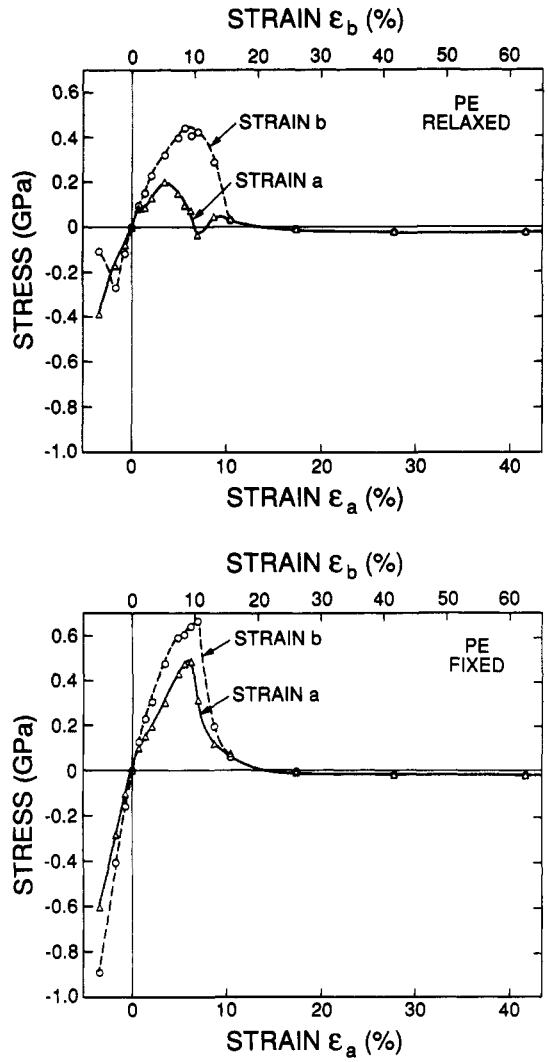

Figure 5. Stress versus strain for finite deformation in the *a* and *b* directions of polyethylene crystal (MCXX *n*-butane force field). Cell parameters perpendicular to the deformation direction are optimized in (a, top) and fixed in (b, bottom).

as the system enters a nonlinear regime. This is reminiscent of the properties of any ductile material, where Young's modulus is constant up to the yield stress σ_y. At this point, plastic deformation begins and the modulus decreases with further strain until the ultimate stress (σ_{ult}) is reached where the sample fractures.

Because we fix the cell dimension along the strain direction, there are small negative stresses at large distances. Optimization of all cell parameters at such distances gives zero stresses without changing the energy significantly.

In Figure 6, strains in the direction perpendicular to the deformation are shown at each finite strain in the *a* (a) and *b* (b) directions. In Figure 6a, when the cell is compressed along a direction (negative strain), the cell is stretched in the *b* direction (positive strain). Conversely, when the cell is stretched in the *a* direction, the cell is compressed in the *b* direction. After the surface is created, the strain in the *b* direction approaches zero as strain in the *a* direction is increased. Similar behavior is observed in Figure 6b except that *a* and *b* are interchanged. In both cases, we find that the strain in the *c* direction is very small (less than 0.05%).

We also carried out calculations in which the cell parameters perpendicular to the deformation direction are fixed. The result is shown in Figure 5b. The stress at each point changes significantly and the position of the peak is also changed. The ultimate stresses are not calculated as 0.48 GPa at 6.2% strain in the *a* direction and 0.66 GPa at 10.4% strain in the *b* direction. The yield stresses are 0.10 and 0.23 GPa.

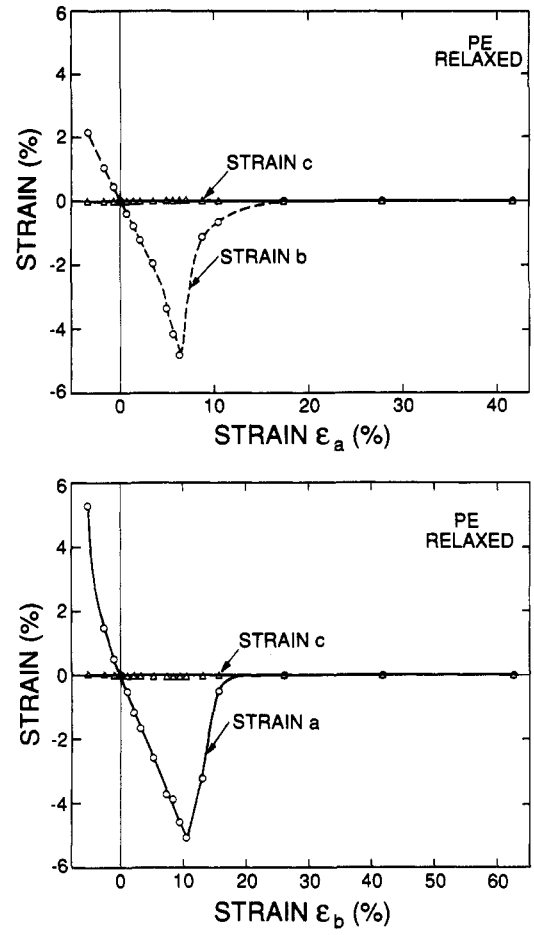

Figure 6. Strain in the perpendicular direction versus strain in the deformation direction. Here cell parameters perpendicular to the deformation direction are optimized. (a, top) Deformation along *a* direction; (b, bottom) deformation along *b* direction.

A particularly interesting behavior is found in the deformation along the *a* direction at a distance of 1.8–2.0 Å. At these distances, stresses become small, but a surface is not created, indicating that the energy is near a stationary point. Starting with the structure at 7.3% strain and using conjugate gradients to optimize all cell parameters and atomic coordinates, we obtain a new extended structure at which forces and stresses vanish! It has an orthorhombic unit cell with a = 7.727 Å, b = 4.483 Å, and c = 2.547 Å. The energy is 0.0931 kcal/mol higher than the optimized structure in Table IV per unit cell (four CH_2 groups). The elastic constant matrix calculated at this structure is

$$\mathbf{C} = \begin{bmatrix} 8.1 & 13.0 & 4.0 & 0 & 0 & 0 \\ 13.0 & 8.0 & 4.4 & 0 & 0 & 0 \\ 4.0 & 4.4 & 338.2 & 0 & 0 & 0 \\ 0 & 0 & 0 & 6.1 & 0 & 0 \\ 0 & 0 & 0 & 0 & 5.6 & 0 \\ 0 & 0 & 0 & 0 & 0 & 6.3 \end{bmatrix} \text{GPa} \qquad (27)$$

The matrix is not positive-definite [$(C_{12})^2 \sim 2C_{11}C_{22}$ leads to a negative eigenvalue], showing that the structure is mechanically unstable.

B. Surface Energy. In Figure 7, the energies are plotted as functions of distance with (a) and without (b) relaxing cell parameters perpendicular to the deformation direction. In Figure 7, the energy varies quadratically near zero and rises monotonically to a constant value for large distances. Since the slabs do not interact for large deformations, the surface energy E_s was calculated by

$$E_s = \frac{E_{def} - E_{eq}}{2S} \qquad (28)$$

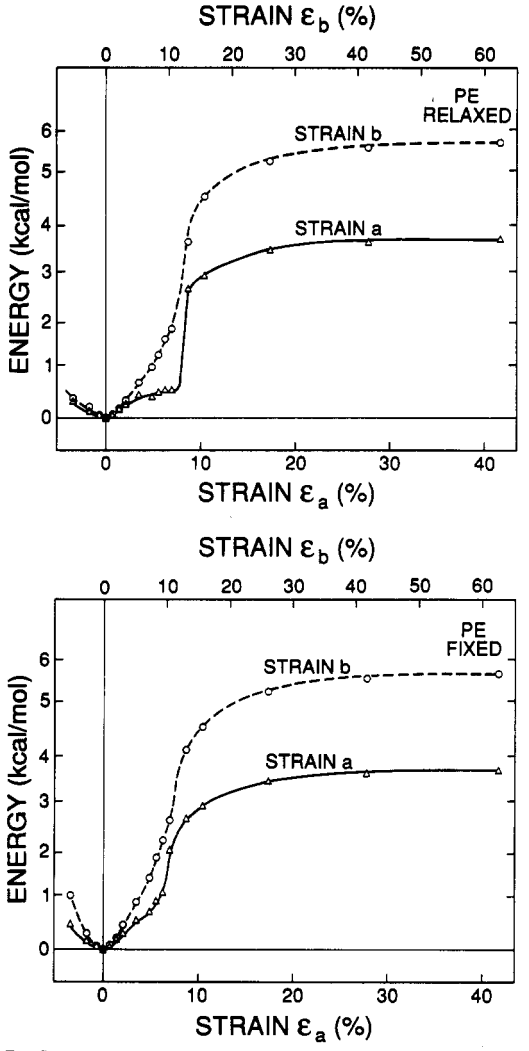

Figure 7. Energy versus strain for finite deformation in the *a* and *b* directions of polyethylene crystal (MCXX *n*-butane force field). Cell parameters perpendicular to the deformation direction are optimized in (a, top) and fixed in (b, bottom).

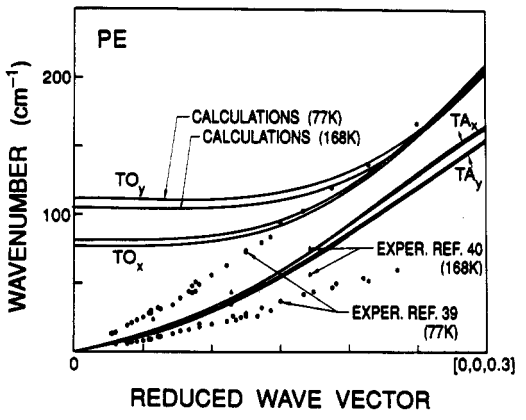

Figure 8. Transverse acoustic and optical bands of PE [using cell parameters at 77 K and 168 K. The circles indicate experimental data of Olf and Fanconi (ref 39) at 77 K, and triangles indicate experimental data of Vergoten et al. (ref 40) at 168 K.

where E_{def} is the energy of the fully deformed cell and E_{eq} is that of the equilibrium cell. Here S is the original area of the unit cell perpendicular to the strain direction, and we take into account that two surface are created.

This leads to a surface energy of 106.8 dyn/cm for the *a* direction [creating the (100) surface] and 109.2 dyn/cm for the *b* direction [creating the (010) surface]. When the (100) surface is created (deformation along the *a* axis), there are two CH_2 groups per unit cell in the new surface cell. Thus the surface energy per CH_2 is $^1/_4$ of the total energy increase or 0.938 kcal/mol. On the other hand, when the (010) surface is created (deformation along the *b* axis), there are four CH_2 groups per new surface cell. Thus the surface energy per CH_2 is $^1/_8$ of the energy change or 0.720 kcal/mol.

If the interactions were nearest-neighbor fiber–fiber only, one would expect the surface energy to be $^1/_3$ the bulk cohesive energy (or 0.683 kcal/mol) for both (100) and (010). This is reasonably close to the calculated values, indicating that such simple models may give useful first estimates.

The calculated surface energies neglect zero-point-energy effects, but this correction should be much smaller than that of lattice energy calculation. Since the calculated cohesive energy for bulk PE is within 2% of the experimental value, we expect our calculated surface energy to have similar accuracy.

An experimental surface energy for low-density PE has been obtained by using the contact angle measurements.[35] The experimental value of 33.1 dyn/cm is about one-third of our calculated values. This suggests that the surface of low-density PE is quite disordered.

TABLE XII: Cell Parameters and Elastic Constants (in GPa) of Polyethylene from Various Calculations

parameter	expt[f] (4 K)	current calcns[e]	other calculations SLB[a]	WB[b]	OM[c]	TKT[d]
a	7.121	7.202	7.05	7.156		
b	4.851	4.795	4.94	4.894		
c	2.546	2.548	2.544			
θ, deg	41 ● 1	41.9	43.1	43.68		
C_{11}		14.0	14.3	13.8	9.27	7.99
C_{22}		13.5	12.2	12.5	10.93	9.92
C_{33}		338.9	341	325	257.4	316
C_{12}		7.9	7.2	7.34	3.68	3.28
C_{13}		2.1	1.92	2.46	3.36	1.13
C_{23}		4.8	3.30	3.96	6.67	2.14
C_{44}		5.3	3.64	3.19	3.46	3.19
C_{55}		3.0	2.27	1.98	1.27	1.62
C_{66}		5.9	7.3	6.24	4.99	3.62

[a] Reference 36. [b] Reference 37. [c] Reference 29. [d] Reference 38. [e] MCXX from *n*-butane. [f] Reference 13.

TABLE XIII: Comparison of Theoretical and Experimental Frequencies (cm^{-1}) for the Accordion (Raman) Mode for *n*-Alkanes (C_nH_{2n+2})

n	theory (MCXX)	experiment least squares[a]	liquid[b]	solid[b]
4	424	473	429 (5)	425 (4)
5	402	411	400 (7)	406 (3)
6	372	358	370 (4)	373 (3)
7	305	313	310 (6)	311 (5)
8	278	278	279 (5)	283 (3)
9	243	249	248 (3)	249 (2)
10	225	225	230 (3)	231 (3)
11	198	206		
12	189	189	195 (1)	194 (2)
13	177	175		
14	163	163		
15	153	153		
16	143	144		140 (3)

[a] Based on the analytic least-squares fit to the observed frequencies (m = 1) as reported in ref 27. [b] Reference 42.

VIII. Comparison with Other Calculations

The cell parameters and elastic constants are compared with other calculated values in Table XII.

Recently, Sorensen et al.[36] (SLB) have obtained the optimized structures and properties of polymer crystals utilizing simultaneous inter- and intramolecular energy minimization. They have used parameters optimized for the polyethylene and poly(oxymethylene)

(35) Owens, D. K.; Wendt, R. C. *J. Appl. Polym. Sci.* **1969**, *13*, 1741.
(36) Sorensen, R. A.; Liau, W. B.; Boyd, R. H. *Macromolecules* **1988**, *21*, 194–199, 200–208.

and calculated properties at the optimized structure of these crystals.

As can be seen from Table XII, there is good agreement between our elastic constants and those of SLB.

The elastic constants of PE have also been obtained theoretically by Odajima and Maeda (OM),[29] Wobser and Blasenbrey (WB),[37] and Tashiro et al. (TKT),[38] as listed in Table XII. The values from WB are in reasonable agreement with our values and those of SLB. However, the elastic constants obtained by OM and by TKT do not agree well with other calculated elastic constants, especially for components perpendicular to the chain directions (C_{11}, C_{22}, C_{12}, C_{66}). This is probably because they used an unreasonably small cutoff distance (4 Å) for the intermolecular interactions.

The vdW parameters of SLB are slightly modified from those of Williams, while the vdW parameters of WB were adjusted to fit the energy and cell parameters of PE. The setting angles of these calculations are 1.2° and 1.8° larger than ours, which is in turn 0.9° larger than experiment.

IX. Summary

Force field parameters adequate for molecular mechanics calculations for PE crystal are developed and tested. Valence force field parameters are obtained by using a theoretical Hessian as well as experimental data for *n*-butane. Nonbond parameters are determined empirically from graphite and PE crystals. The cell and atomic coordinate optimizations were carried out on PE crystal, and elastic constants and phonon bands were calculated by using analytical second derivatives. To examine the behavior of the crystal under large strain in the directions perpendicular to the chain, stress and energy are plotted as functions of deformation distances. Yield stresses and surface energies are calculated from these relations.

Acknowledgment. This work was partially supported by grants from the Air Force Office of Scientific Research (No. AFOSR-88-0051), the Caltech Consortium in Chemistry and Chemical Engineering, and Imperial Chemical Industries, Wilton Materials Research Centre, Cleveland, England.

Registry No. Polyethylene (homopolymer), 9002-88-4.

(37) Wobser, G.; Blasenbrey, S. *Kolloid Z. Z. Polym.* **1970**, *241*, 985.
(38) Tashiro, K.; Kobayashi, M.; Tadokoro, H. *Macromolecules* **1978**, *11*, 914.
(39) Olf, H. G.; Fanconi, B. J. *Chem. Phys.* **1973**, *59*, 534.
(40) Vergoten, G.; Fleury, G.; Tasumi, M.; Shimanouchi, T. *Chem. Phys. Lett.* **1973**, *19*, 191.
(41) Wu, C-K.; Nicol, M. *J. Chem. Phys.* **1973**, *58*, 5150.
(42) Mizushima, S.; Shimanouchi, T. *J. Am. Chem. Soc.* **1948**, *71*, 1320.

Basis Set Effects on the Intermolecular Interaction Energies of Methane Dimers Obtained by the Møller–Plesset Perturbation Theory Calculation

Seiji Tsuzuki* and Kazutoshi Tanabe

National Chemical Laboratory for Industry, Tsukuba, Ibaraki 305, Japan (Received: February 28, 1990)

Intermolecular interaction energies of methane dimer were calculated by using several basis sets up to 6-311G(3d,4p) with electron correlation energy correction by the Møller–Plesset perturbation method and basis set superposition error (BSSE) correction by the counterpoise method to evaluate the basis set effect. The calculated interaction energies depended on the basis set considerably. Whereas the interaction energies of repulsive component calculated at HF level were not affected by the change of basis set, the dispersion energy component depended greatly on the basis set used. The dispersion energies calculated with the Møller–Plesset second- and third-order perturbation by using 6-311G(2d,2p) basis set were 0–10% and 4–6% smaller than those obtained with the fourth-order (MP4(SDTQ)) perturbation, respectively. The BSSE's calculated by the counterpoise method were still about 30% of the calculated intermolecular interaction energies for the conformers of energy minima even at the MP4(SDTQ)/6-311G(2d,2p) level. The calculated interaction potentials of dimers at the MP4(SDTQ)/6-311G(2d,2p) level were considerably shallower than those obtained by MM2 force fields but were close to the potentials given by the Williams potential and by the recently reported MM3 force field.

Introduction

The nonbonded interactions of carbon and hydrogen atoms are important to understand the intramolecular and intermolecular interactions of organic molecules. These interactions frequently play a crucial role in the determination of the conformation of molecule and crystal structure.[1,2] These interactions have attracted much attention from chemists and have been studied by various methods. The intermolecular interaction potential of methane has been estimated from the measurement of compressibility of gaseous methane.[3-9] The intermolecular interactions of organic molecules have also been investigated from the analysis of crystal structure and lattice energy.[10-15]

A simple empirical representation of the intermolecular interaction energy is a sum of pairwise additive atom–atom interaction energy terms with each term being the sum of several energy components. The atom–atom interaction energy term can be described as

$$E(\text{total}) = E(\text{repulsion}) + E(\text{dispersion}) + E(\text{Coulombic}) \quad (1)$$

A lot of equations have been proposed to describe the atom-atom interaction energy term.[16-18] The parameters of the equations,

(1) Burkert, U.; Allinger, N. L. *Molecular Mechanics*; American Chemical Society: Washington, DC, 1982.
(2) Dale, J. *Stereochemistry and Conformational Analysis*; Verlag Chemie; New York, 1978.
(3) Schamp, Jr., H. W.; Mason, E. A.; Richardson, A. C. B.; Altman, A. *Phys. Fluids* **1958**, *1*, 329.
(4) Dymond, J. H.; Rigby, M.; Smith, E. B. *J. Chem. Phys.* **1965**, *42*, 2801.
(5) Snook, I. K.; Spurling, T. H. *J. Chem. Soc., Faraday Trans. 2* **1972**, *68*, 1359.
(6) Hanley, H. J. M.; Klein, M. *J. Phys. Chem.* **1972**, *76*, 1743.
(7) Pope, G. A.; Chappelear, P. S.; Kobayashi, R. *J. Chem. Phys.* **1973**, *59*, 423.
(8) Matthews, G. P.; Smith, E. B. *Mol. Phys.* **1976**, *32*, 1719.
(9) Sherwood, A. E.; Prausnitz, J. M. *J. Chem. Phys.* **1964**, *41*, 429.
(10) Williams, D. E.; Starr, T. L. *Comput. Chem.* **1977**, *1*, 173.
(11) Bates, J. B.; Busing, W. R. *J. Chem. Phys.* **1974**, *60*, 2414.
(12) Lii, J.-H.; Allinger, N. L. *J. Am. Chem. Soc.* **1989**, *111*, 8576.
(13) Warshel, A.; Lifson, S. *J. Chem. Phys.* **1970**, *53*, 582.
(14) Sprague, J. T.; Allinger, N. L. *J. Comput. Chem.* **1980**, *1*, 257.
(15) Allinger, N. L.; Miller, M. A.; VanCatledge, F. A.; Hirsch, J. A. *J. Am. Chem. Soc.* **1967**, *89*, 4345.
(16) Lennard-Jones, J. E. *Proc. R. Soc. London, Ser. A* **1924**, *106*, 463.
(17) Buckingham, A. D.; Utting, B. D. *Annu. Rev. Phys. Chem.* **1970**, *21*, 287.

0022-3654/91/2095-2272$02.50/0